Volume 12
Number 22
14 June 2024
Pages 5263–5562

Journal of Materials Chemistry B

Materials for biology and medicine

rsc.li/materials-b

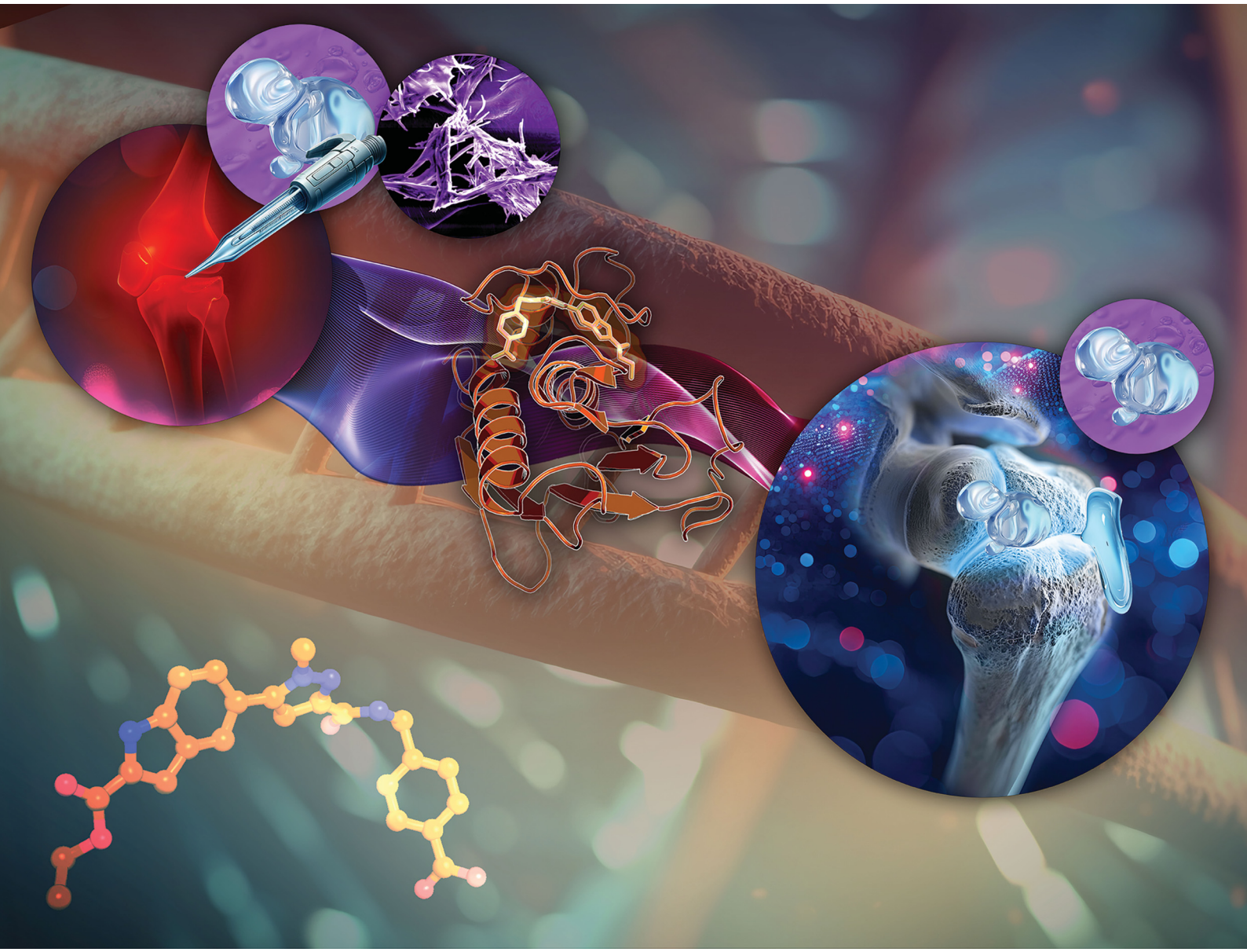

ISSN 2050-750X

ROYAL SOCIETY OF CHEMISTRY

PAPER

Deepa Ghosh *et al.*

On-demand release of a selective MMP-13 blocker from an enzyme-responsive injectable hydrogel protects cartilage from degenerative progression in osteoarthritis

Journal of Materials Chemistry B

ROYAL SOCIETY OF CHEMISTRY

PAPER

View Article Online
View Journal | View Issue

Cite this: J. Mater. Chem. B, 2024, 12, 5325

On-demand release of a selective MMP-13 blocker from an enzyme-responsive injectable hydrogel protects cartilage from degenerative progression in osteoarthritis†

Himadri Shekhar Roy,[a] Preethi Murugesan,[a] Chirag Kulkarni,[b] Malika Arora,[a] Geet Kumar Nagar,[b] Rajdeep Guha,[c] Naibedya Chattopadhyay[b] and Deepa Ghosh*[a]

In osteoarthritis (OA), the degradation of cartilage is primarily driven by matrix metalloprotease-13 (MMP-13). Hence, the inhibition of MMP-13 has emerged as an attractive target for OA treatment. Among the various approaches that are being explored for MMP-13 regulation, blocking of the enzyme with specific binding molecules appears to be a more promising strategy for preventing cartilage degeneration. To enhance effectiveness and ensure patient compliance, it is preferable for the binding molecule to exhibit sustained activity when administered directly into the joint. Herein, we present an enzyme-responsive hydrogel that was designed to exhibit on-demand, the sustained release of BI-4394, a potent and highly selective MMP-13 blocker. The stable and compatible hydrogel was prepared using triglycerol monostearate. The efficacy of the hydrogel to prevent cartilage damage was assessed in a rat model of OA induced by anterior cruciate ligament transection (ACLT). The results revealed that in comparison to the rats administrated weekly with intra-articular BI-4394, the hydrogel implanted rats had reduced levels of inflammation and bone erosion. In comparison to untreated control, the cartilage in animals administered with BI-4394/hydrogel exhibited significant levels of collagen-2 and aggrecan along with reduced MMP-13. Overall, this study confirmed the potential of BI-4394 delivery using an enzyme-responsive hydrogel as a promising treatment option to treat the early stages of OA by preventing further cartilage degradation.

Received 5th December 2023,
Accepted 17th April 2024

DOI: 10.1039/d3tb02871b

rsc.li/materials-b

1. Introduction

The primary functions of articular cartilage (AC) located in joints include absorption of impact, minimize load on the underlying bone, and reduce friction between the joint surfaces. The extracellular matrix (ECM) of AC is mostly composed of water (70–80%), collagens (10–25%) and proteoglycans (PGs, 5–15%). The avascular cartilage contains chondrocytes embedded in the ECM.[1–3] The avascular nature and low cell density limit its regenerative potential. Damage to AC leads to osteoarthritis (OA), a debilitating disease that affects a large number of people worldwide.[4–6] In the United States alone, 151 million individuals are reported to be affected by the disease.[7,8] The existing pharmacological treatment of OA is purely symptomatic, and does not prevent further degeneration of the cartilage.[9] The key players in OA progression are matrix metalloproteinases (MMPs), which are responsible for the ECM destruction.[10–12] Based on their structure and substrate, the cartilage degrading MMPs are termed as collagenases (MMP-1, MMP-8 and MMP-13).[13,14] Among these, MMP-13 (collagenase-3) has the highest specificity and efficiency to cleave collagen II, the major matrix protein present in cartilage.[15,16] In addition, increased levels of MMP-13 have proved to play a catabolic role in OA patients.[17–20] Numerous studies have focused on the creation and assessment of chemical compounds that can inhibit MMPs.[21] However, the structural similarity among the active sites of MMPs has resulted in their failure in clinical trials due to their lack of selectivity and undesirable musculoskeletal side effects, including inflammation and joint stiffness known as muscular skeletal syndrome (MSS).[22,23]

[a] Chemical Biology Unit, Institute of Nano Science and Technology, Knowledge City, Sector-81, Mohali-140306, Punjab, India. E-mail: deepa.ghosh@inst.ac.in
[b] Division of Endocrinology and Centre for Research in ASTHI, CSIR-Central Drug Research Institute, Lucknow–226031, Uttar Pradesh, India
[c] Division of Laboratory Animal Facility, CSIR-Central Drug Research Institute, Lucknow–226031, Uttar Pradesh, India

† Electronic supplementary information (ESI) available: Cytocompatibility studies, gene expression studies, hydrogel characterization, rheology, *in-vivo* serum biochemical analysis (LFT and KFT), *in-vivo* OARSI scoring and *in-vivo* MMP-13 level estimation. See DOI: https://doi.org/10.1039/d3tb02871b

Consequently, pharmaceutical research has primarily concentrated on the identification of powerful MMP-13 inhibitors that exhibit a strong selectivity to MMP-13 over other MMPs.[24,25] Recently MMP-13 inhibitors that bind selectively to the less conserved S1′ pocket of MMPs, are designed for improved specificity.[26–31] One such molecule is 4-[({5-[2-(ethoxycarbonyl)-1*H*-indol-5-yl]-1-methyl-1*H*-pyrazol-3-yl}formamido)methyl]-benzoate (BI-4394), an indole-based inhibitor that was developed by Boehringer Ingelheim to selectively bind to the S1′ pocket of MMP-13. *In silico* interaction studies and X-ray crystallography studies confirmed the binding affinity of BI-4394 with MMP-13 (RCSB PDB I.D: 5BPA). In comparison to MMP-13 (> 1000-fold), it has lower activity against other matrix metalloproteinases: MMP-1 (IC-50 > 22 μM), MMP-2 (18 μM), MMP-3 (> 22 μM), MMP-7 (> 22 μM), MMP-8 (> 22 μM), MMP-9 (8.9 μM), MMP-10 (16 μM), MMP-12 (> 22 μM) and MMP-14 (8.3 μM). *In vitro* studies showed that BI-4394 selectively blocks the MMP-13 activity with an IC-50 value of 0.001 μM.[32]

In comparison to a systemic route of drug administration, the intra-articular (IA) route has a number of advantages, including improved local bioavailability, reduced systemic drug exposure, less adverse events and reduced cost.[33–36] Recently, the efficacy of deuterated pyrimidine dicarboxamide, a MMP-13 inhibitor was assessed after administering the molecule IA weekly.[29] Repeated IA administration as a result of low drug residence time will result in patient non-compliance due to multiple visits to the hospital, discomfort, infection risk and high cost.[36,37] The administration of a formulation that enables sustained release of a drug would improve patient compliance and reduce the cost of treatment.[38–41] Multiple platforms such as micelles, solid lipid nanoparticles (SLN), polymeric microparticles and hydrogels are reported for the sustained release of drugs in the joints. Such systems were generally used for the intra-articular delivery of disease-modifying OA drugs (DMOADs), glucocorticoids and non-steroidal anti-inflammatory drugs (NSAIDs) and cell-based therapies.[42–48] However, no sustained delivery system has been reported so far with a MMP-13 inhibitor.

BI-4394 has been reported to block MMP-13 with high specificity and potency. While the molecule was shown to inhibit *ex-vivo* bovine nasal cartilage degradation, no *in vivo* studies have been reported.[32] With the aim of improving its bioavailability, herein, we report the development of an enzyme-responsive hydrogel for the sustained release of BI-4394 using FDA approved triglycerol monostearate (TG-18) as a self-assembling amphiphilic hydrogelator. TG-18 is a cost-effective, small-molecule amphiphile known for its safety and is recognized as a Generally Recognized as Safe (GRAS) compound by the Food and Drug Administration (FDA). Due to its ability to self-assemble during the heating/cooling process, it can encapsulate a wide range of therapeutic agents.[49–51] Moreover, this hydrogel features an enzyme-cleavable linker, enabling disassembly in response to enzymes found in an inflammatory environment and supports the sustained release of the drugs to match the severity of inflammatory conditions, thus optimizing therapeutic efficacy while reducing toxicity.[52,53] Since the ester linkages present in the hydrogel could be cleaved by an enzyme having esterase activity and facilitate its disassembly, we chose TG-18 as a gelator for the sustained release of BI-4394. *In vitro* studies confirmed the sustained release of BI-4394 from the hydrogel with those enzymes that are frequently detected in OA joints. The *in vivo* efficacy of the BI-4394-loaded hydrogel to prevent cartilage degeneration was evaluated in a rat OA model achieved by anterior cruciate ligament transection (ACLT).

2. Experimental section

2.1. Materials

Reagents including solvents like HPLC water and DMSO were obtained from commercial suppliers (TCI-India and Merck). Triglycerol monostearate (TG-18) was purchased from AK Scientific, India. BI-4394 (molecular weight: 446.5 g mol^{-1}) and Recombinant Human MMP-13 protein (R&D Biosystems) were a kind gift from Boehringer Ingelheim Pharma. Recombinant human MMP-8 protein and a MMP fluorogenic substrate were purchased from R & D Biosystems, USA. Porcine liver esterase and a dialysis membrane (7 kDa) were obtained from Sigma-Aldrich, USA. DMEM, collagenases-II, cell culture materials, QPCR kits, primary and secondary antibodies were obtained from Thermo Fischer Scientific, USA.

2.2. Isolation of human articular chondrocytes

Human articular chondrocytes were harvested from discarded cartilage samples obtained from donors after informed consent as per the protocol approved by the Institutional Ethics Committee of PGIMER, Chandigarh (IEC-08/2017-659). The chondrocytes were isolated as per the published protocol.[54] Briefly, the samples were decontaminated using alcohol and antibiotic cocktail and digested with collagenase II solution in DMEM at 37 °C for 12 h. After digestion, the medium was passed through a 70 μm cell strainer, and the filtrate was centrifuged to separate chondrocytes. The sediment was washed with DPBS to remove enzymes and was again centrifuged. The pellet was dispersed in a chondrocyte growth medium (CGM) (Lonza, US) and transferred to T-25 flasks. Chondrocytes were cultured in a humidified incubator supplied with 5% CO_2 at 37 °C. The experiments were conducted using chondrocytes of passage numbers 3–4.

2.3. Cytocompatibility assay of BI-4394

The cytocompatibility of BI-4394 was confirmed using the isolated chondrocytes. In brief, the chondrocytes were seeded in a 96-well plate at a cell density of 4000 cells per well and incubated for 24 h in CGM media and then treated with different concentrations of BI-4394 for 48 h at 37 °C in a 5% CO_2 incubator in DMEM media. The viability of the cells was checked using the 3-(4,5-dimethylthiazol-2-YL)-2,5-diphenyltetrazolium bromide (MTT) Assay. The absorbance of the formazan crystals was measured at 575 nm using a spectrophotometer (Tecan Infinite M Plex).[55] The cell viability was

calculated using the following equation:

$$\%\,\text{Viability} = \frac{\text{Abs. of treated cells}}{\text{Abs. of control cells}} \times 100 \quad (1)$$

2.4. Determination of NF-κB p65 translocation

NF-κB plays a central role in inflammatory conditions. It can be activated by different stimuli that can further up-regulate various other pro-inflammatory genes. In order to understand the molecular mechanism of BI-4394 on NF-κB activation under inflammatory conditions, immunofluorescence analysis was performed using IL-1β-activated chondrocytes. The activation of the NF-κB pathway was observed using antibodies raised against p65, a subunit of NF-κB. Briefly, chondrocyte cells were seeded on a chamber slide at a cell density of 10^4 cells per wells. After 24 h, the cell was treated with IL-1β alone (10 ng mL^{-1}) and along with BI-4394 (25 μM) for 6 h. Untreated chondrocytes served as a control group. Post-incubation, the treated chondrocytes were washed with PBS, fixed with 4% paraformaldehyde, permeabilized with 0.1% Triton X-100 for 10 min, and blocked with 1% BSA for 1 h. The cells were then incubated with the NF-κB p65 sub-unit primary antibody (1 : 300) overnight at 4 °C followed by incubation with a goat anti-rabbit superclonal recombinant secondary antibody tagged with Alexa Fluor 568 (1 : 1000) for 3 h at room temperature (RT). The cells were then washed in PBS and the nucleus was stained with Hoechst and imaged using a confocal microscope.[56]

2.5. Gene expression assay

In order to evaluate the effect of BI-4394 on gene regulation, gene expression by BI-4394 was evaluated under inflammatory conditions using qPCR. The mRNA expression was evaluated for the following genes using the respective primers: IL-1β (Hs00174131_m1), MMP-13 (Hs00233992_m1), TNF-α (Hs00174128_m1), iNOS (Hs01075529_m1), COL-2A (Hs00164004_m1), SRY-Box Transcription factor 9-SOX-9 (Hs00164004_m1) and Aggrecan – ACAN (Hs00202971_m1) using the Taqman gene expression assay (Applied Biosystems). Briefly 1.5 × 10^6 cells per wells were seeded in a 6-well plate. The chondrocytes were stimulated with IL-1β (10 ng mL^{-1}) along with BI-4394 (5 μM and 25 μM), respectively. Untreated chondrocytes served as the control. Total RNA was isolated using the PureLink RNA Mini Kit (Ambion, by Life Technologies) following the manufacturer's protocol. The purity and concentration of the RNA were assessed using a Nanoquant, and then the RNA was reverse transcribed into cDNA using Applied Biosystems, Thermo Scientific equipment. Subsequently, the cDNA, along with qPCR mix, primers, and ddH_2O, was amplified in a qPCR system (Quant3 Studio, Applied Biosystems, Thermo Scientific). Amplification conditions included incubation at 50 °C for 2 minutes, initial denaturation at 95 °C for 10 minutes, followed by 40 cycles of denaturation at 95 °C for 15 seconds and annealing/extension at 50 °C for 1 minute. The expression levels of various samples were normalized using the 2(−ΔΔCt) method with GAPDH (Hs00204173_m1) as the reference gene.[54]

2.6. *In vitro* evaluation of MMP-13 inhibition

BI-4394 was tested for MMP-13 inhibition activity using the MMP fluorogenic substrate (QXL520-γ-Abu-Pro-Cha-Abu-Smc-His-Ala-Dab(5-FAM)-Ala-Lys-NH2 (Smc = *S*-methyl-L-cysteine)) according to the manufacturer's protocol (R&D Biosystem). Briefly, different concentrations of BI-4394 were dissolved in DMSO and were added to the MMP fluorogenic substrate (20 μM) in a black 96-well plate. An equal amount of MMP-13 enzyme (10 ng) was added to each well and incubated at 37 °C for 90 min in a multimode plate reader in the kinetics mode (Tecan Infinite M Plex). A test reaction, without BI-4394 served as control. The fluorescence intensity of the MMP substrate was quantified at excitation/emission (320 nm/405 nm) wavelength.[32] Similarly, the specificity of BI-4394 (10 μM) was checked with different MMPs (10 ng), including MMP-8 (Collagenase-II), Gelatinase – (MMP-2 and MMP-9) respectively.

2.7. Synthesis of the hydrogel

To prepare the hydrogel, 100 mg of triglycerol monostearate (TG-18) was weighed in a glass vial and heated to 65–85 °C until it melted. BI-4394 (5 and 10 mg) dissolved, respectively, in DMSO (0.2 mL) was added to the melted TG-18 followed by water (0.8 mL) making the total volume to 1 mL and the final DMSO: water volume ratio 1 : 4. The respective gels were designated as Gel@5 and Gel@10, respectively. A blank formulation was prepared in a similar way, without BI-4394 (Gel@0). The respective vials were cooled to room temperature, resulting in a hydrogel formation. Gelation was considered complete when no gravitational flow was observed upon inversion of the vial.[51]

2.8. Encapsulation and loading efficiency

The hydrogels were centrifuged at 5000 rpm for 10 min to calculate the entrapped BI-4394. The supernatant and sediment were separated, and the BI-4394 concentration in the supernatant was determined by UV analysis. The calibration curve of BI-4394 was plotted with its maximum absorption wavelength recorded at 310 nm. The entrapped molecule was calculated with the help of the standard curve of BI-4394. The encapsulation and loading efficiency were calculated using the given formulas:[57]

$$\text{Total entrapped BI-4394} = (\text{Total BI-4394 added} - \text{BI-4394 in supernatant}) \quad (2)$$

$$\text{BI-4394 loading}\,\% = \frac{\text{Entrapped BI-4394 in hydrogel}}{\text{Amount of TG-18}} \times 100 \quad (3)$$

$$\text{Encapsulation efficiency}\,\% = \frac{\text{Entrapped BI-4394 in hydrogel}}{\text{Total amount of BI-4394}} \times 100 \quad (4)$$

2.9. Hydrogel characterization

The morphology of the hydrogels was evaluated using a microscope (Olympus). The hydrogels were lyophilized and their structural morphology was further confirmed by high resolution FE-SEM (JEOL JSM-7610 F Plus).[51] Fourier transform infrared

(FT-IR) spectroscopy was used to confirm the encapsulation of BI-4394 in the hydrogels. The FT-IR spectrum was recorded by ATR using VERTEX 70 FT-IR (Bruker, US) from 2000 to 500 cm^{-1} at 4 cm^{-1} resolution.

2.10. Rheological and mechanical properties of the hydrogel

Rheological characterization of the hydrogel was conducted using a modular rheometer (AntonPaar, Austria), using plate geometry (PP-25). The changes in the storage modulus (G') and the loss modulus (G'') from 65 °C to 25 °C were measured at a fixed frequency of 1 Hz and a heating/cooling rate of 5 °C min^{-1}. Frequency sweep experiments were carried out in a frequency range of 0.1–100 rad s^{-1} at 25 °C and 0.1% strain. To evaluate injectability, the viscosity of both the blank hydrogel (Gel@0) and the BI-4394-hydrogel (Gel@10) was measured before and after injection at 25 °C in a frequency range of 0.1–100 rad s^{-1}.[53]

2.11. Cytocompatibility of the hydrogel

The compatibility of the cells with the hydrogel was assessed using its trans-well insert.[54,58] Briefly, 5000 chondrocytes were seeded in 96 well plates containing trans-well inserts. After culturing overnight, the medium was replaced with fresh medium, fresh medium with 50 μL Gel@0 hydrogel and fresh medium with 50 μL Gel@10 hydrogel was added to the upper chamber and incubated for a period of 48 h at 37 °C. An equivalent amount of free BI-4394 was used as a control group.[51] Post-incubation, the seeded chondrocytes were washed with PBS and the cell viability was evaluated using MTT as reported in Section 2.4.

2.12. *In vitro* release of BI-4394 from the hydrogel

The enzyme-responsive release of BI-4394 from the TG-18 hydrogel was performed at pH 7.4 and at 37 °C using a dialysis bag.[51] Briefly, a known amount of BI-4394 loaded hydrogels was suspended in PBS (200 mL) and was incubated with porcine liver esterase (100 U mL^{-1}) in the activated dialysis membrane (7 kDa molecular weight cut off) with stirring at 100 rpm.[51] For evaluating the stability, the hydrogel was incubated with and without the esterase (200 U mL^{-1}). In order to confirm the esterase-dependent release of BI-4394, Gel@10 was incubated with two concentrations of esterase (100 and 200 U mL^{-1}) and its release was studied.[51,59] In another set of experiments, to check whether MMPs can cleave the ester bonds in TG-18 to release BI-4394, Gel@10 was incubated with recombinant human MMP-9 (1.5 μg mL^{-1}) and recombinant human MMP-13 (10 ng mL^{-1}), respectively. To mimic the OA inflammatory conditions, fresh enzymes were added at set time points. At each time interval, 1 mL of the sink media was removed and replaced with fresh PBS. The concentration of BI-4394 in the aliquoted sample was analysed by UV absorbance at 310 nm and calculated through a standard curve.

2.13. Stability of BI-4394 in the hydrogel

The stability of the hydrogel was evaluated after incubating Gel@10 at 4 °C, and 37 °C for two months. After the incubation, Gel@10 was disrupted through a sonicator and the released BI-4394 was quantified using UV absorbance. The activity of entrapped BI-4394 released from the hydrogel was assessed by comparing its MMP-13 inhibitory activity with an equal amount of freshly prepared BI-4394. The MMP-13 inhibition was assessed by the MMP fluorogenic substrate as mentioned previously in Section 2.2.

2.14. *In vivo* studies

All animal studies were performed as per the guidelines laid out by the committee for the purpose of control and supervision of experiments on animals (CPCSEA), Government of India and approved by the Institutional Animal Ethics Committee (IAEC) of Central Drug Research Institute, (CDRI) Lucknow (approval No. IAEC/2022/24).

2.14.1. Rat OA model. Forty-two female Sprague–Dawley rats (200–220 g) were randomly divided into seven groups (n = 6 per group). Using the ACLT procedure, we induced OA as it closely depicts human OA conditions.[60,61] Group-1: control, and to develop the model, the rats were anesthetized using xylazine:ketamine (10 : 40 mg kg^{-1}), and the surgery was performed in the right knee of remaining 36 animals. One week post-surgery, the ACLT rats were randomized into the following groups; group 2: rats with ACLT and injected with saline (50 μL); group 3: rats with ACLT and injected with BI-4394 (80 μg) in saline as a single dose (SD); group 4: rats with ACLT and injected with BI-4394 (80 μg) injected as a double dose (DD), administered 15 days after the 1st dose; group 5: rats with ACLT and injected with Gel@0 (50 μL in saline); group 6: rats ACLT and injected with Gel@10 containing BI-4394 (80 μg, SD); and group 7: rats with ACLT and injected with Gel@10 containing BI-4394 (80 μg, DD). At the end of the experiment, all animals were sacrificed and their surgery legs were harvested for further evaluations.[29,61,62]

2.14.2. Gait analysis. The spontaneous mobility of the animals was assessed as described before with slight modifications.[63,64] A walking path was created in a confined compartment with food pellets placed on top of inverted trays located on either side of the path. The animals were provided with only water O/N. On the day of the experiment, the gait and the number of times each individual rat stood on its hind legs to access the food was assessed for a fixed time interval using a video camera. Besides, a digital Vernier calliper was used to measure the bilateral knee joint thickness.[64–66]

2.14.3. *In vivo* biochemical analysis. In order to evaluate the *in vivo* safety of the administered hydrogels, the rat serum was analysed using the liver function test (LFT) and the kidney function test (KFT) using a biochemical analyser (XL-200 – Tranasia) following the supplier kit's protocols (Transasia Bio-Medicals Ltd. India). KFT includes blood urea (Cat no. 121025), creatinine (Cat no. 121022) and urea nitrogen (BUN) (Cat no. 120214) levels. LFT includes serum glutamic-oxaloacetic transaminase (SGOT) (Cat no. 120616), serum glutamic-pyruvic transaminase (SGPT) (Cat no. 120617), alkaline phosphatase (ALP) (Cat no. 121018) and total bilirubin (Cat no. 120621).[67]

These are conducted to assess the health and functionality of the liver and kidneys, respectively.

2.14.4. Micro-CT (μCT) analysis of knee joints. The knee joints were analysed *via* μCT using a Sky Scan 1276 scanner (Sky Scan, Bruker, Belgium). Scanning was performed at a voxel size of 18 μm under a voltage of 70 kV and a current of 200 μA, using a 1.0 mm aluminium filter, 180° rotation with 0.6° rotation steps. The scanned files were reconstructed using the NRecon software. The bone microarchitectural parameters such as bone volume/tissue volume (BV/TV%) and trabecular number (Tb. N) were quantified manually using CTAn software.[61]

2.14.5. Histological analysis. The rat knees were fixed in 4% formalin followed by decalcification and the adjacent muscles around the knee were excised. The decalcified and cleaned knee tissue samples were embedded in paraffin and cut into 5 μm sections. The tissue sections were processed for histological analysis by hematoxylin and eosin (H&E) staining.[61] The collagen content in the respective cartilage was assessed using Masson trichrome staining using the Masson Trichrome Staining Kit (Real Gene). The respective knee joint sections were assessed according to the Osteoarthritis Research Society International (OARSI) guidelines as described in ESI† Table S1.[68,69]

2.14.6. Immunohistochemistry. The tissue sections were rehydrated sequentially with xylene and graded ethanol (100%, 90%, 70%, and 50%) for 5 min each, followed by PBS wash. Antigen retrieval was perfomed using pre-heated 10 mM sodium citrate buffer (pH-6) at 80 °C for 1 min. After incubation, the sections were rinsed with PBS and treated with 3% H_2O_2 solution for 20 min and washed with PBS. Blocking was achieved by immersing the sections in a 4% BSA solution for 2 h at RT. Collagen-II, MMP-13 and aggrecan were stained using specific primary antibodies at 1 : 100 dilution after overnight incubation at 4 °C. Primary antibodies were detected using respective secondary antibodies conjugated with horse radish peroxidase at 1 : 1000 dilution and stained with DAB and counter stained with hematoxylin.[57] The sections were rinsed with PBS, rehydrated, mounted, and analysed using a microscope (Olympus).

2.14.7. *In vivo* evaluation of MMP-13. Quantification of MMP-13 was performed using a specific MMP-13 fluorogenic substrate as per the published protocol.[70] Briefly, the respective rat serum (50 μL) was added to the MMP-13 fluorogenic substrate and was assessed for MMP-13 activity. Fluorescence intensity was measured at (320 nm/405 nm) excitation and emission, respectively (Tecan Infinite M Plex).

2.15. Statistics

Results were expressed as mean ± standard deviation. All data were analyzed using one way analysis of variance followed by Dunnett's multiple comparison test. Values of $p < 0.05$ were considered as significant. All the statistical analyses were performed using graph pad prism 5 software (Graph Pad Software, Inc., San Diego, CA, USA).

3. Results and discussion

3.1. Effect of BI-4394 on chondrocytes

3.1.1. Cytocompatibility of BI-4394. Several molecules that bind specifically to the S1 pocket of MMP-13 have been reported.[27,28] BI-4394 similarly binds to the SI pocket of -MMP-13 and is highly potent. To evaluate its cytocompatibility, BI-4394 (1–250 μM) was added to human articular chondrocytes and its effect on proliferation was studied. BI-4394 had no effect on chondrocyte viability up to 1 μM (Fig. 1A). At higher concentrations >10 μM, the viability was comparatively reduced. A similar response was observed with the morphology of the cells, with lower concentration displaying a morphology similar to that of the untreated control (Fig. S1, ESI†). As the reported IC-50 value of BI-4394 is 1 nm,[32] BI-4394 can be considered cytocompatible.

3.1.2. Effect of BI-4394 on gene expression. The activation of NF-κB, a pro-inflammatory transcription factor is known to induce MMP-13 expression apart from several pro-inflammatory cytokines. Many reports have shown that OA can be mitigated by blocking NF-κB activation.[71–73] To evaluate if BI-4394 can prevent NF-κB activation, BI-4394 was added to interleukin-1β (IL-1β) activated chondrocytes. The translocation of the p65 subunit of

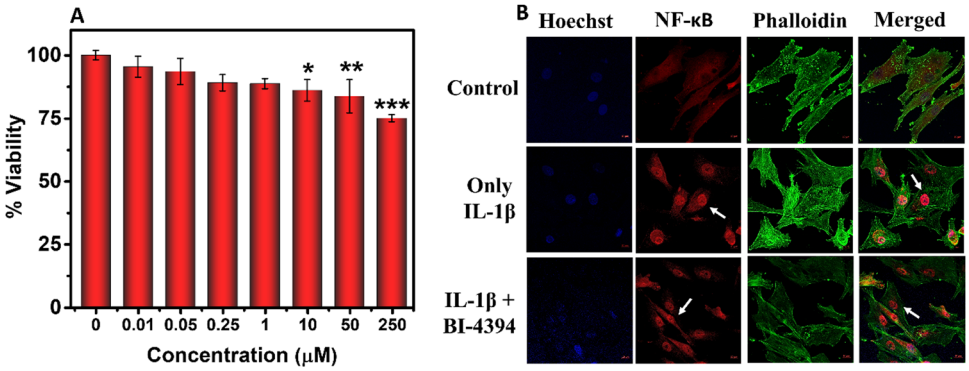

Fig. 1 *In vitro* effect of BI-4394. (A) Proliferation of chondrocytes treated with BI-4394; one-way ANOVA, Dunnett's multiple comparison test. * represents the significant difference in comparison to untreated control. (***$p \leq 0.0001$, **$p \leq 0.01$ and *$p \leq 0.05$). (B) Effect of BI-4394 on NF-κB activation. p65 (red)-positive cells are indicated by white arrows. Nucleus is stained with Hoechst (blue) and the cytoskeleton is stained with phalloidin (green). Images were captured at 20× magnification.

NF-κB from the cytoplasm to the nucleus suggested the activation of the NF-κB pathway (Fig. 1B). The presence of the p65 unit in the nucleus of activated cells treated with BI-4394 suggested that BI-4394 did not block the activation of the NF-κB pathway. MMP-13 is reported to be activated by IL-1β.[71,74] To evaluate the effect of BI-4394 on MMP-13 gene, IL-1β activation in chondrocytes was evaluated by MMP-13 expression using qPCR. The studies revealed that IL-1β treatment resulted in a 250-fold increase in the expression of MMP-13 as compared to untreated control. No change in the expression of MMP-13 with BI-4394 indicated that the molecule had no influence on MMP-13 gene expression (Fig. S2A, ESI†). A similar response observed with other pro-inflammatory genes including tumor necrosis factor (TNF-α) and inducible nitric oxide synthase (iNOS) (Fig. S2, ESI†) confirmed that BI-4394 has no effect on their expression.

3.1.3. Blocking of MMPs by BI-4394. The MMP binding activity of BI-4394 was evaluated using a specific MMP fluorogenic substrate.[32] In this, treatment of the non-fluorescent substrate with a specific MMP that is capable of cleaving the substrate results in the cleavage of the attached quencher to form a fluorogenic substrate. The intensity of the fluorescence is directly proportional to the MMP activity. As shown in Fig. 2A, the addition of MMP-13 (10 ng) to the substrate resulted in a time dependent increase in fluorescence intensity. In contrast, a dose dependent inhibition of the fluorescence intensity was observed in the presence of BI-4394. The lowest concentration (0.156 μM) and the highest tested concentration (5 μM) of BI-4394 reduced the fluorescence intensity to 50% and 10%, respectively, which confirmed the efficiency of BI-4394 to block MMP-13. Similar data were also obtained by Taylor *et al.*, with BI-4394 which showed a IC_{50} of 0.001 μM with a tested concentration of MMP-13 of 125 pM, which re-confirms the MMP-13 binding activity of BI-4394.[32] The activity of BI-4394 (5 μM) was further similarly evaluated using other different classes of MMPs. While BI-4394 showed complete reduction in the fluorescence intensity with collagenase-III (MMP-13), suggesting complete inhibitory activity, similar studies conducted with collagenase-II (MMP-8) revealed only 30% inhibition (Fig. 2B). In contrast, no significant inhibition was observed with gelatinases (MMP-2 and MMP-9) (Fig. 2C), which confirmed the specificity of BI-4394 towards MMP-13.

3.2. Development of an enzyme-responsive hydrogel

3.2.1. Synthesis of BI-4394 loaded hydrogel. Although BI-4394 is highly potent and specific to MMP-13,[32] its limited solubility and stability in water would be a challenge for clinical development. To overcome the limitations, we entrapped the molecule in a self-assembling amphiphilic hydrogelator and evaluated its efficacy under *in vitro* and *in vivo* conditions.

The hydrogels were prepared by heating a mixture of BI-4394 in DMSO, TG-18 and water. An opaque hydrogel was formed on cooling (Fig. S3A, ESI†). Two different concentrations of BI-4394 (5 and 10 mg mL^{-1}) were used in the hydrogel formation and designated as Gel@5 and Gel@10, respectively. In the blank hydrogel, only DMSO was added (Gel@0). Microscopic examination of the hydrogels revealed that the blank gel contained numerous spherical structures (Fig. 3A, a and b), while BI-4394 containing hydrogels had fibre-like structures. In comparison to Gel@5, the density of the fibre-like structures was more in Gel@10 (Fig. 3A, c–f). A similar observation was noted in the FE-SEM study, with a greater number of long fibre-like structures in Gel@10 than in Gel@5 (Fig. 3A, h and i). Similar structures were observed in TG-18 hydrogels by Joshi *et al.* and Chen *et al.* used for the encapsulation of Triamcinolone acetonide and Rosiglitazone, respectively.[51,53] The encapsulation efficiency of BI-4394 in Gel@5 and Gel@10 was 65% w/w and 85% w/w, respectively, suggesting considerable encapsulation of BI-4394 in the TG-18 hydrogel. The increase in the density of the needle-like structures is ascribed to an increase in the entrapment of BI-4394. The encapsulation of BI-4394 was confirmed with FTIR studies wherein similar peak shifting was observed in both Gel@5 and Gel@10 in comparison to the blank gel (Fig. S3B, ESI†).

3.2.2. Cytocompatibility study of the BI-4394 loaded hydrogel. The cytocompatibility of the hydrogel was investigated by comparing the proliferation of the chondrocytes with the contact media obtained from the respective hydrogels. As shown in Fig. 3B, the proliferation of the cells exposed to the hydrogel was comparable with the proliferation of the cells treated with control and BI-4394, suggesting the biocompatibility of the hydrogel. In addition, the morphology of the treated cells was similar to the control cells, confirming the cytocompatibility of the respective hydrogels (Fig. S4, ESI†).

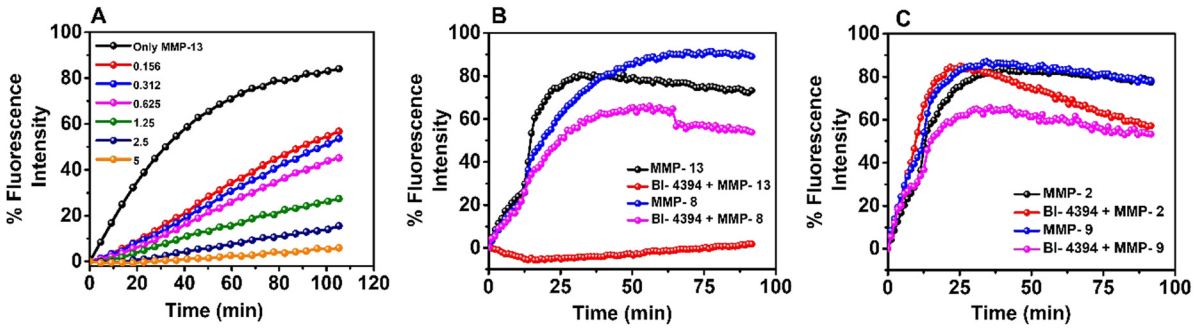

Fig. 2 Blocking of MMPs by BI-4394 using the MMP fluorogenic substrate. (A) Dose dependent inhibition of MMP-13 by BI-4394; specificity of BI-4394 among different classes of MMPs. (B) Collageneases (MMP-8 and MMP-13) and (C) gelatineases (MMP-2 and MMP-9).

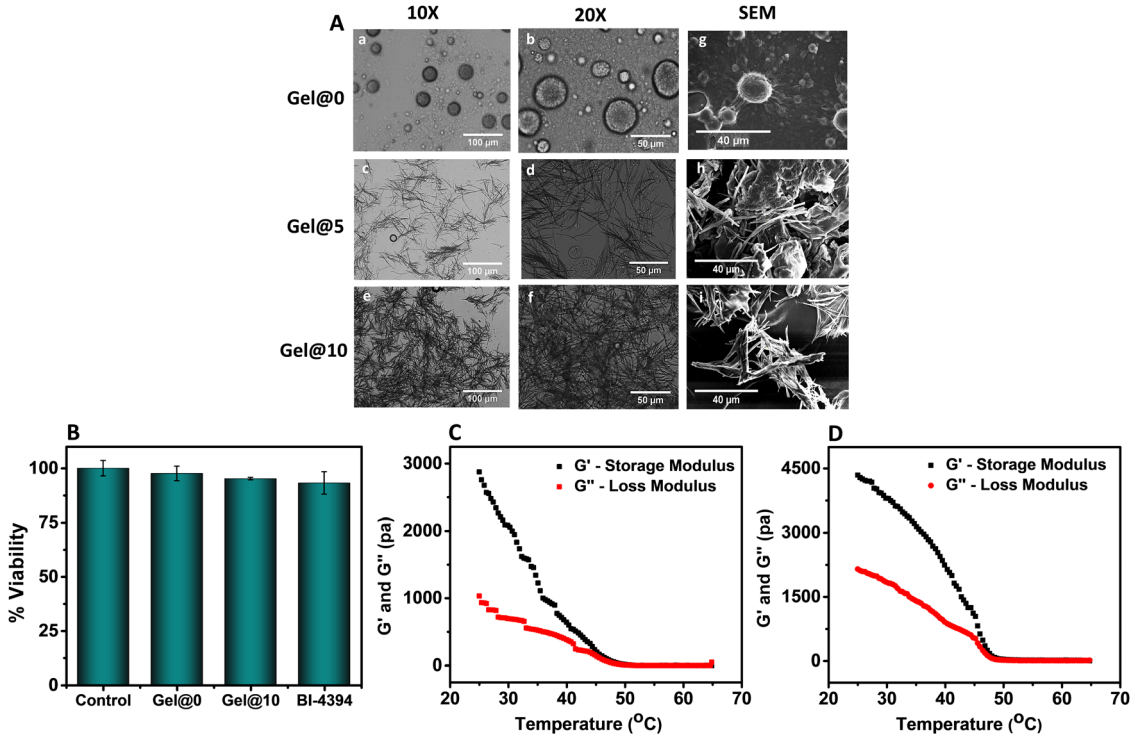

Fig. 3 Characterization of the BI-4394 loaded hydrogel. (A) Morphology of the hydrogel. (a)–(f) Microscopic images of respective hydrogels at 10× (Scale bar represents 100 μm) and 20× magnification (Scale bar represents 50 μm); (g)–(i) FE-SEM images of hydrogel (Scale bar represents 40 μm); (B) viability of chondrocytes using trans-well assay with respective hydrogels; temperature sweep studies; (C) blank hydrogel (Gel@0); and (D) BI-4394 loaded hydrogel (Gel@10).

3.2.3. Rheology. The rheological properties of the hydrogel were investigated using a rheometer. The gel to sol transition was observed in the temperature sweep studies carried out from 65 °C to 25 °C. As the temperature reduced, the storge modulus G' increased rapidly, the gelation temperature of $G' = G''$ was 48.12 °C for the Gel@0 hydrogel (Fig. 3C) and 50 °C for the Gel@10 hydrogel (Fig. 3D). Gel@10 exhibited a much higher storage modulus than Gel@0, indicating stiffening of the hydrogel due to BI-4394 encapsulation. A similar observation was made by Chen *et al.*, using Rosiglitazone.[53] The frequency sweep experiments with both the hydrogels revealed an increase in the G' values throughout the frequency sweep, signifying the formation of a stable hydrogel (Fig. S5A and B, ESI†). The injectability of the respective hydrogels was confirmed using the shear viscosity frequency sweep measurement. A decrease in the viscosity after injection throughout the frequency sweep from 0.1 to 100 rad s^{-1} confirmed the shear thinning characteristic of the hydrogel which enables it to pass through the needle (Fig. S5C, ESI†).

3.2.4. Release profile of the BI-4394 loaded hydrogel. Apart from the MMPs, esterase is detected in the synovial fluid of OA patients.[75–77] Since the ester bonds present in TG-18 are susceptible to esterase and MMPs, we used it to achieve sustained release of BI-4394.[51] To investigate the release of the encapsulated BI-4394 in response to the enzymes, Gel@5 and Gel@10 were placed in dialysis bags containing 100 U mL^{-1} esterase. In order to mimic the *in vivo* flare conditions, fresh enzyme was periodically added to the dialysis solution. In the presence of enzyme, 95% and 80% of BI-4394 were released from Gel@5 and Gel@10, respectively, for 30 days, suggesting the sustained release of BI-4394 (Fig. 4A). Given the high encapsulation efficiency and favourable release kinetics of Gel@10, this hydrogel was used in all further studies.

To check the specificity of release, the release of BI-4394 from Gel@10 was determined with and without esterase. Whereas Gel@10 incubated in PBS alone showed 20% cumulative release over a period of 30 days, the hydrogel incubated with esterase showed a 80% release confirming the release of BI-4394 was on account of breakage of the esterase bond in TG-18 (Fig. 4B). Moreover, to check whether the BI-4394 release is dependent on the concentration of enzyme, Gel@10 was incubated with two different concentrations of esterase (100 and 200 U mL^{-1}). An increase in the BI-4394 release observed with the higher concentration of enzyme suggested that the hydrogel was capable of releasing BI-4394, "on-demand", with the release being dependent on the concentration of the enzyme (Fig. 4C). These data confirm that the release of BI-4394 is dependent on the enzyme concentration present in the milieu. A similar observation was made by Joshi *et al.*, using a TG-18 hydrogel, in which they reported 80% release of the encapsulated drug in 30 days with esterase treatment in comparison to the absence of an enzyme.[51] To investigate the release of BI-4394 from Gel@10 in the presence of MMPs that are released in OA, Gel@10 was incubated with MMP-9 and MMP-13,

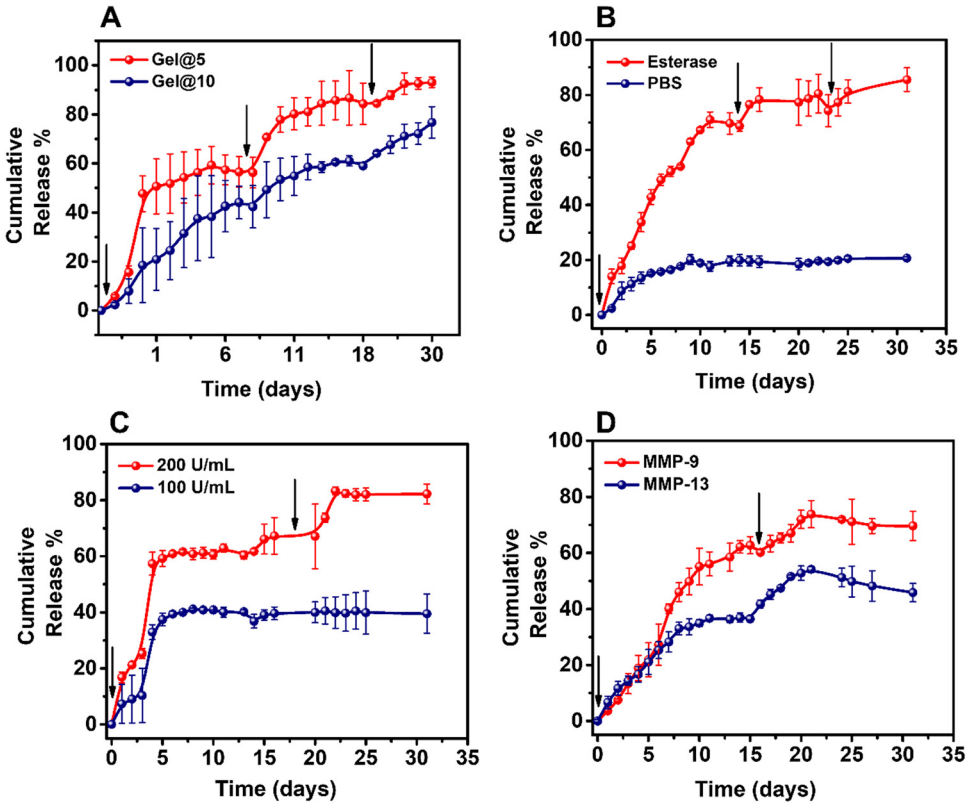

Fig. 4 Release of BI-4394 from the hydrogel. (A) BI-4394 release from the respective hydrogels in the presence of esterase (100 U mL^{-1}); (B) BI-4394 release from Gel@10 in the presence and absence of esterase (200 U mL^{-1}); (C) esterase dependent BI-4394 release from Gel@10; and (D) release of BI-4394 from Gel@10 in the presence of MMP-9 (1.5 μg mL^{-1}) and MMP-13 (10 ng mL^{-1}), respectively.

respectively. The enzyme concentration was chosen based on the enzyme concentration reported in the synovial fluid of arthritic patients.[51,78,79] The results showed 75% release of BI-4394 from the hydrogel upon incubation with MMP-9, while only 45% was released with MMP-13. This difference can be attributed to the blocking of MMP-13 activity by the released BI-4394 which suggests the efficacy of the released BI-4394 to block MMP-13 (Fig. 4D).

3.2.5. Stability study of the BI-4394 hydrogel. As the stability of the entrapped BI-4394 is critical for its application, we evaluated its stability in Gel@10. The activity of the entrapped BI-4394 was evaluated as reported in Section 2.13. Data revealed that the activity of the entrapped BI-4394 was similar to that of the freshly prepared BI-4394, suggesting the stability of the BI-4394 in the hydrogel (Fig. 5).

3.3. In vivo studies

The ability of specific MMP-13 blocking molecules to prevent cartilage degeneration have been reported using a rapid cartilage-degrading inflammatory model (MIA model).[29,30] In this study, we had used the ACLT model, as it induces degradation of the articular cartilage that affects the weight bearing ability and

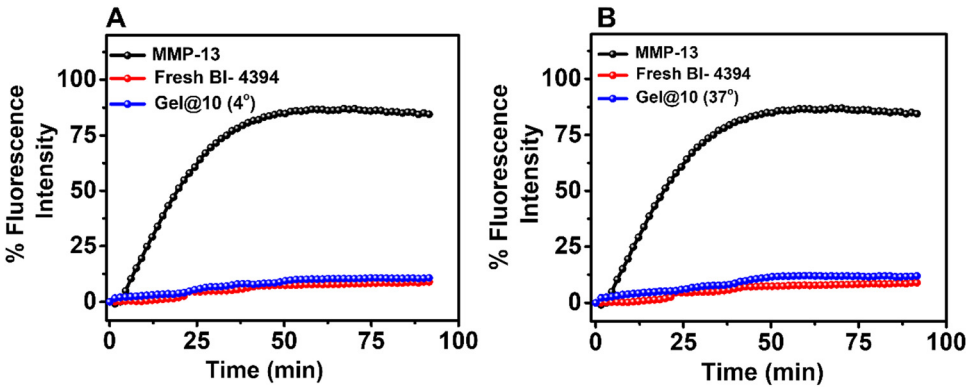

Fig. 5 *In vitro* stability and MMP-13 inhibition activity of the Gel@10 hydrogel at different temperatures. (A) 4 °C; (B) 37 °C.

mobility of the animals, with the outcome being similar to that observed in post-traumatic human OA.[61,80–83] Studies have shown that the ACLT model exhibits changes in the cartilage and the underlying bone at the early stages of ligament transection.[62,81,82,84,85] The efficacy of the BI-4394 loaded hydrogel to prevent cartilage degradation through MMP-13 blocking was evaluated in an *in vivo* model. Post ACLT, the test animals were implanted with Gel@10 as a single dose (SD) or a double dose (DD) through IA administration, to determine the effective dose for therapeutic efficacy. Similarly, BI-4394 was administered in the respective ACLT-operated group as shown in the schematic representation (Fig. 6A). With the aim of comparing the outcome of SD and DD of free-BI-4394, we chose to similarly administer the Gel@10 as SD and DD, respectively. At the end of the study, the gait and standing posture of the animals were evaluated. The gait of an OA animal is affected due to inadequate load-bearing ability in the affected knee. The mechanical stress and prolonged wear and tear of OA joint lead to cartilage degeneration and OA progression. The walking pattern therefore provides critical information on ambulatory biomechanics. We observed that the rats in the ACLT and Gel@0 groups had a dragging gait in their right hind leg after the surgery. However, in the groups treated with either a SD or DD of BI-4394 or Gel@10, the rats exhibited a normal walking pattern, similar to that of the healthy control group. The ability of the rats to stand on their hind limbs was assessed by the number of times they stood on the hind limbs to access the food during a fixed time interval. The quantified data shown in Fig. 6B revealed that animals injected with Gel@10 exhibited significant recovery and was comparable to that of healthy animals. In contrast, the animals injected with BI-4394 (SD and DD) did not exhibit similar effect. Furthermore, the thickness of the knee also revealed that Gel@10 was more efficient than free BI-4394 (Fig. 6C).

No change in the body weight was observed among all the rats' groups during the dosing duration (data not shown). Moreover, the *in vivo* safety data revealed no systemic change was observed in LFT and KFT levels among all the groups confirming the *in vivo* safety of the administered hydrogels (Fig. S6, ESI†).

At the knee joint, the cartilage and subchondral bone work as a single osteochondral unit and play complementary roles in load-bearing of the joints.[83,86] While the cartilage reduces friction during motion, the subchondral bone supports the overlying cartilage and distributes the mechanical load across the joint surface.[87,88] In OA, along with progressive loss of articular cartilage, the subchondral bone damage is observed.[61] Visual evaluation of the excised joint revealed a smooth surface in the healthy group. In contrast, the surface in ACLT and Gel@0 implanted rats exhibited damage in the OA joint. In comparison, the animals administered with BI-434 (SD and DD) and animals implanted with Gel@10 (SD and DD)

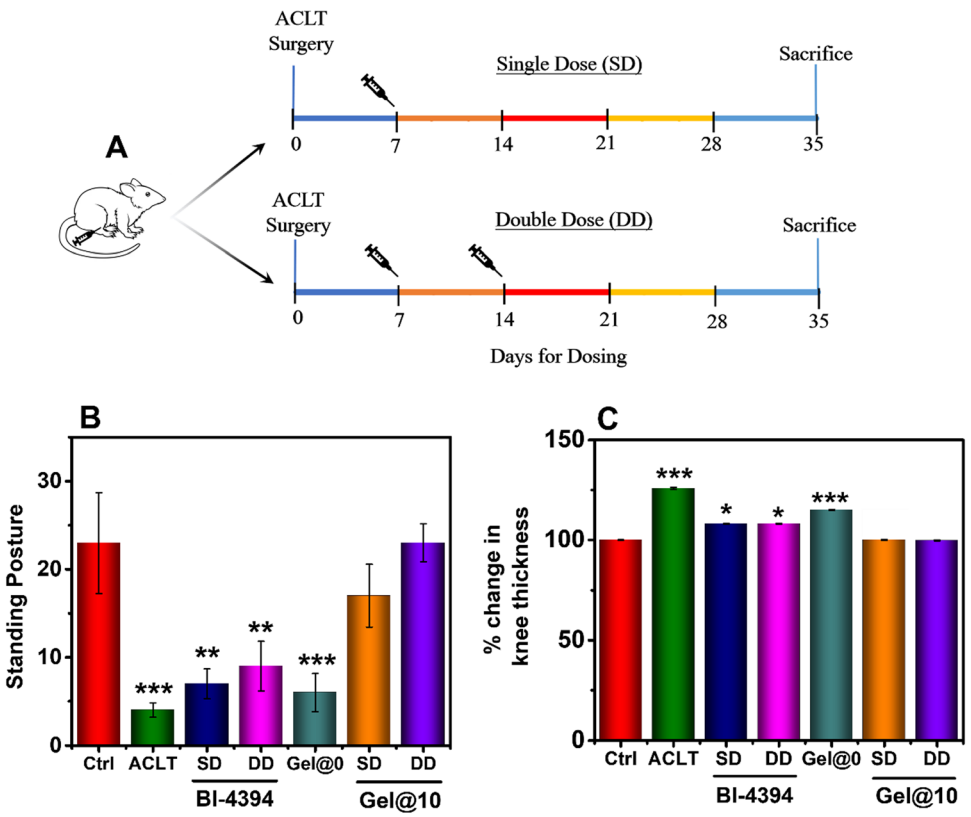

Fig. 6 *In vivo* studies of the BI-4394 loaded hydrogel. (A) Dosing pattern for the treatments; (B) quantification of standing position on their hindleg after treatment. (C) % Change in the knee thickness of rat after treatment. One-way ANOVA, Dunnett's multiple comparisons test. * Represents a significant difference compared to the control (ctrl) group. (***$P \leq 0.0001$, **$P \leq 0.01$ and *$P \leq 0.05$).

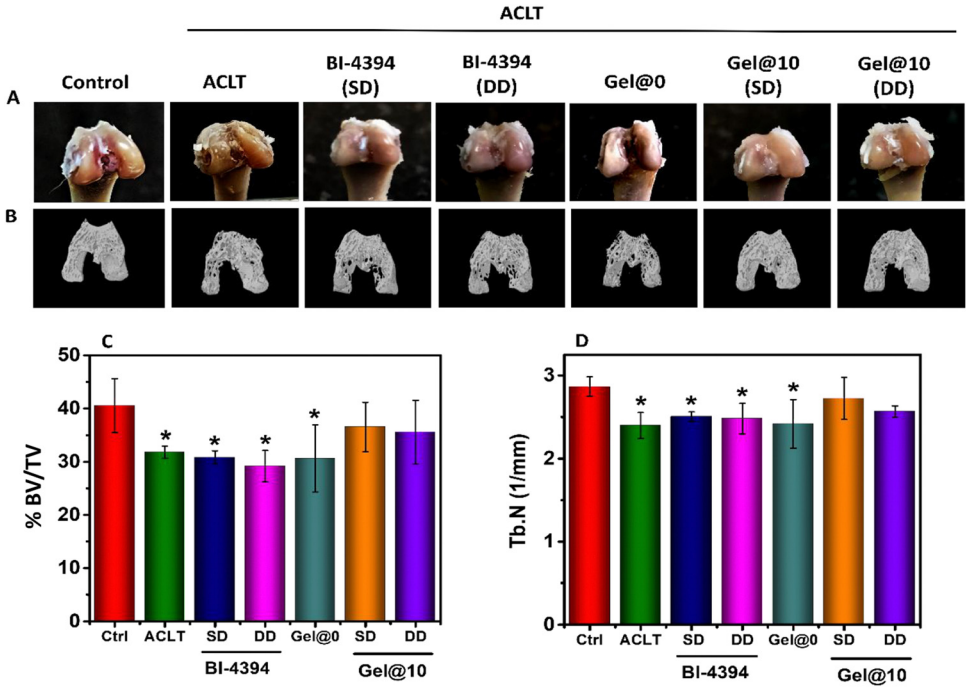

Fig. 7 Structural analysis of ACLT knee treated with BI-4394. (A) Gross morphology; (B) μCT data, μCT analysis; (C) quantitate analysis of treated knee; (C) bone volume (BV)/tissue volume (TV); and (D) trabecular number (Tb. N). One-way ANOVA, Dunnett's multiple comparisons test. * Denotes the significance in comparison to the control (ctrl) group. (*$p < 0.05$).

exhibited a smooth surface similar to that of the control group (Fig. 7A). Further μ-CT analysis was done to evaluate the sub-chondral bone. 3D images revealed changes in the microarchitecture of sub-chondral bone in ACLT and Gel@0 in comparison to the healthy group. The animals administered with BI-43 (SD and DD) revealed an improved architecture as compared to ACLT and Gel@0. The animals implanted with Gel@10 exhibited a microarchitecture which was comparable to that of healthy group (Fig. 7B), suggesting that early administration of the MMP-13 inhibitor is beneficial in preventing further cartilage degeneration.

Bone volume density, represented as BV/TV%, indicates the percentage of bone volume to tissue volume. The trabecular number (Tb. N) is the measure of the average number of trabeculae per unit length. BV/TV% and trabecular number (Tb. N) were calculated from the μCT analysis.[89] As shown in Fig. 7C and D, there was a significant reduction in the BV/TV% and Tb. N in the ACLT, Gel@0 and free BI-4394 (SS and DD) groups, in comparison to the control group. No significant changes were observed in the case of Gel@10 (SS and DD), indicating the protective role of the BI-4343 loaded hydrogel over free BI-4394. Furthermore, the absence of any difference between the SD and DD of Gel@10 suggested that a single dose was adequate to prevent cartilage degeneration.

Histological assessment of the rat knee was performed using hematoxylin and eosin (H&E) staining. Similar to the changes observed in the gross morphology, cartilage damage in the ACLT model was observed in the OA joint (Fig. 8A and B). A similar observation was seen with the Gel@0 group. In comparison, rats administered with BI-4394 (SD and DD) exhibited intact cartilage. However, the Gel@10 implanted animals displayed a thick intact cartilage that was comparable to the cartilage in the control group (Fig. 8A and B). This was further confirmed with Masson Trichrome staining in which the collagen content in the matrix is represented by the intense blue matrix. An intense blue colour was observed in Gel@10 (SD and DD) which was comparable to that of the control group, whereas in the free BI-4394 (SD and DD), the intensity was remarkably reduced, suggesting that Gel@10 prevented the degradation of collagen present in the cartilage in comparison to free BI-4394 (Fig. 8C). The assessment of the sections as per the OARSI soring guidelines revealed significant degeneration of the knee in the ACLT (Score 3.5) and Gel@0 (Score 3.2) groups. While the administration of free BI-4394 in the knees had scores of 2.8 (SD) and 2.0 (DD), the scores were 0.89 (SD) and 0.84 (DD) in rats implanted with Gel@10 that were comparable to that of the control group (Score 0.681) (Fig. S7, ESI†). The improvements observed in animals implanted with Gel@10, in comparison to direct BI-4394 administration, could be due to its better bioavailability.

To further confirm the status of articular cartilage specific proteins such as collagen-2 (COL-2A) and aggrecan (AGCN), immunohistochemistry (IHC) analysis was done using tissue sections. Free BI-4394 administered animals exhibited higher expression of COL-2A and AGCN with DD showing a comparatively higher expression than SD. The expression of these proteins in Gel@10 (SD and DD) was comparable to that of control groups suggesting that Gel@10 was more effective than free BI-4394 (Fig. 9A and B). Moreover, the levels of protein expressed between Gel@10 (SD and DD) was comparable

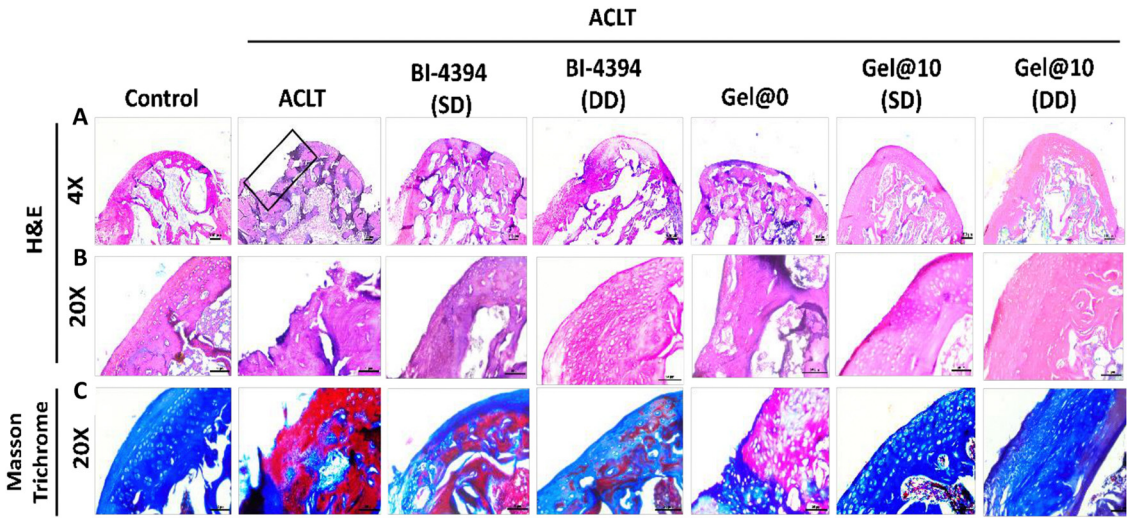

Fig. 8 Histological assessment of rat right hind knee. (A) H&E staining (4× magnification); (B) higher magnification (20×) of the damaged area as highlighted in the box; and (C) Masson trichrome staining of the damaged area (20×).

suggesting that the single hydrogel dose is as effective as the double dose. A similar pattern was observed in the Masson trichrome staining. Furthermore, we checked MMP-13 expression in tissue sections as shown in Fig. 9C. MMP-13 was highly expressed in ACLT and Gel@0. The expression was considerably down in free BI-4396 (SD and DD). The expression of MMP-13 in Gel@10 (SD and DD) was comparable to that of the control group proving that Gel@10 is more effective than free BI-4394 in preventing cartilage degeneration (Fig. 9C).

The assessment of MMP-13 activity in the respective rat serum using a specific fluorogenic substrate demonstrated high levels of MMP-13 in ACLT and Gel@0 groups (Fig. S8, ESI†). In comparison, the MMP-13 levels were less in all the treatment groups with the inhibition being more significant in Gel@10 (SD and DD) groups. The significant reduction in the serum levels of MMP-13 in rats treated with Gel@10 could be either due to the inhibition in the progression of cartilage degeneration or blocking of MMP-13 activity, or both. Although the histological and immunological data (Fig. 8 and Fig. 9) support the earlier statement that the lower levels of MMP-13 in animals treated with Gel@10 are due to the protection of the cartilage from progressive degeneration that results in subsequent reduction in MMP-13 expression; the efficient MMP-13 binding activity of BI-4394 released from the hydrogel could also prevent its detection in the serum.

As the purpose of testing Gel@10 as SD and DD regimens was to determine the effective therapeutic regimen,[90,91] the results clearly indicate the efficacy of SD to be comparable to DD in preventing cartilage degeneration. The cartilage of the OA-rats in which the Gel@10 was administered as a SD was comparable to that of the control (non-OA group), suggesting that this dosing regimen was sufficient to mitigate the OA conditions. The absence of a discernible difference in response between SD and DD suggests that a dose-dependent *in vivo* response was not apparent in this case. This preclinical observation underscores the robustness of the therapeutic effect

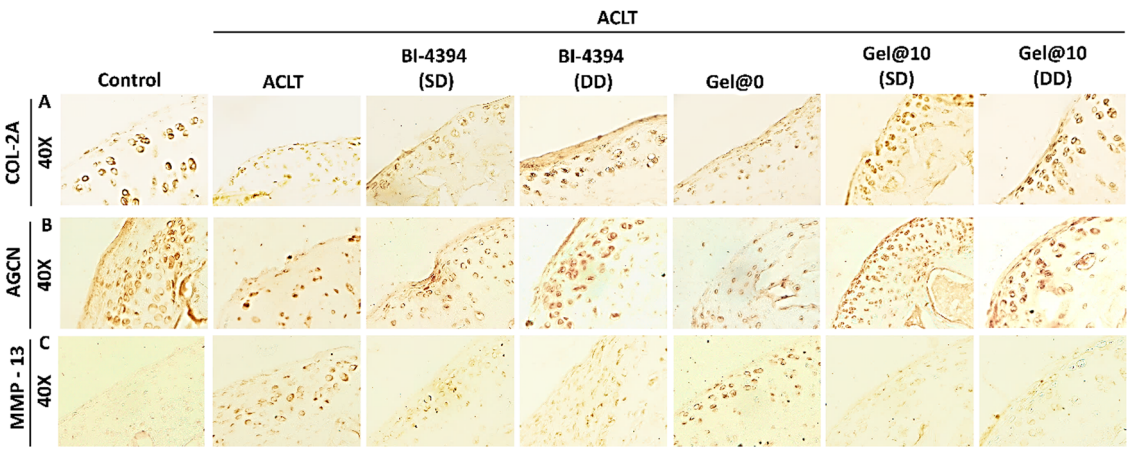

Fig. 9 Immunohistochemistry (IHC) staining of respective tissue in the right hind knee. (A) Collagen-2 (COL-2A) staining; (B) aggrecan (AGCN) staining; and (C) MMP-13 staining. Images were captured at 40× magnification.

achieved with the SD regimen and supports the adoption of a SD regimen for future clinical trials. Given the comparable OA mitigating response to DD, the SD regimen offers the benefits of reduced treatment burden and improved patient compliance. This study confirms the advantage of delivering BI-4394 from the TG-18 hydrogel, which is specifically responsive to esterase enzymes and undergoes disassembly to release adequate BI-4394 to block MMP-13 activity, thereby preventing further cartilage degradation.

4. Conclusion

Herein, we studied the potential of BI-4394, a selective MMP-13 inhibitor, to protect cartilage from degeneration. The cytocompatible BI-4394 had no influence on NF-κB, nor on the expression of pro-inflammatory genes that are implicated in cartilage degeneration. In comparison to other metalloproteases, BI-4394 exhibited efficient binding to MMP-13 and blocked its bioactivity. The long-term stability of BI-4394 was enabled by encapsulating the molecule in an enzyme-responsive hydrogel. *In vitro* studies revealed improved stability of BI-4394 following its encapsulation in an enzyme-responsive hydrogel. The hydrogel exhibited release of BI-4394 in the presence of enzymes such as MMP-13 and esterase, confirming the enzyme-responsive, on-demand release. In comparison to direct intra-articular administration of free BI-494, administration of the BI-4394 using the enzyme-responsive hydrogel was more effective in protecting the cartilage from degeneration. The results confirm the prophylactic potential of MMP-13 inhibitors in preventing the progress of cartilage degeneration. From the clinical perspective, our approach to release the MMP-13 inhibitor using an enzyme-responsive, injectable hydrogel is clinically attractive as it is likely to have better patient compliance.

Author contributions

HSR: conceptualization, data curation, formal analysis, investigation, methodology, and writing – original draft; PM, CK, MA, and GKN: formal analysis, investigation, methodology, and visualization; RG: supervision, methodology, and visualization; NC: supervision, funding acquisition, and writing – review and editing; and DG: conceptualization, supervision, funding acquisition, writing – review and editing, and project administration.

Conflicts of interest

The authors declare no conflict of interest.

Acknowledgements

DG acknowledges SERB for funding (CRG/2018/000213, SPF/2021/000151). NC acknowledges SERB: SPR/2019/000346 and CSIR: MLP-2035 for funding. We thank opnMe.com the open innovation website of Boehringer Ingelheim for providing free of charge the MMP-13 inhibitor (BI-4394) and recombinant human MMP-13 protein (https://www.opnme.com/molecules/mmp13-bi-4394), Dr Sameer Aggarwal, PGIMER, Chandigarh, is acknowledged for providing cartilage samples. CK thanks CSIR, India for research fellowship. Mumuksha Yadav is acknowledged for her help with the *in vitro* studies. We thank Anurag Basu from CDRI, Lucknow for LFT and KFT studies.

References

1 D. R. Eyre, *Semin. Arthritis Rheum.*, 1991, **21**, 2–11.
2 D. R. Eyre, M. A. Weis and J.-J. Wu, *Eur. Cell Mater.*, 2006, **12**, 57–63.
3 H. Muir, P. Bullough and A. Maroudas, *J. Bone Jt. Surg., Br. Vol.*, 1970, **52**, 554–563.
4 A. J. Sutherland, G. L. Converse, R. A. Hopkins and M. S. Detamore, *Adv. Healthcare Mater.*, 2015, **4**, 29–39.
5 M. Tschaikowsky, S. Brander, V. Barth, R. Thomann, B. Rolauffs, B. N. Balzer and T. Hugel, *Acta Biomater.*, 2022, **146**, 274–283.
6 W. Wei, Y. Ma, X. Zhang, W. Zhou, H. Wu, J. Zhang, J. Lin, C. Tang, Y. Liao, C. Li, X. Wang, X. Yao, Y. W. Koh, W. Huang and H. Ouyang, *ACS Appl. Mater. Interfaces*, 2021, **13**, 54801–54816.
7 S. Brown, S. Kumar and B. Sharma, *Acta Biomater.*, 2019, **93**, 239–257.
8 A. Mobasheri and M. Batt, *Ann. Phys. Rehabil. Med.*, 2016, **59**, 333–339.
9 J. Steinmeyer, F. Bock, J. Stöve, J. Jerosch and J. Flechtenmacher, *Orthop. Rev. (Pavia)*, 2018, **10**(4), 7782.
10 M. B. Goldring and S. R. Goldring, *Ann. N. Y. Acad. Sci.*, 2010, **1192**, 230–237.
11 G. Murphy and M. H. Lee, *Ann. Rheum. Dis.*, 2005, **64**, 44–47.
12 E. U. Sumer, B. C. Sondergaard, J. C. Rousseau, P. D. Delmas, A. J. Fosang, M. A. Karsdal, C. Christiansen and P. Qvist, *Osteoarthr. Cartil.*, 2007, **15**, 212–221.
13 H. S. Roy, G. Dubey, V. K. Sharma, P. V. Bharatam and D. Ghosh, *J. Biomol. Struct. Dyn.*, 2022, **40**, 2339–2351.
14 Z. Lei, M. Jian, X. Li, J. Wei, X. Meng and Z. Wang, *J. Mater. Chem. B*, 2020, **8**, 3261–3291.
15 E.-S. E. Mehana, A. F. Khafaga and S. S. El-Blehi, *Life Sci.*, 2019, **234**, 116786.
16 R. Phillips, *Nat. Rev. Rheumatol.*, 2021, **17**, 645.
17 C. Milaras, P. Lepetsos, D. Dafou, M. Potoupnis, E. Tsiridis, C. Milaras, P. Lepetsos, D. Dafou, M. Potoupnis and E. Tsiridis, *Cureus*, 2021, **13**(10), e18607.
18 Q. Hu and M. Ecker, *Int. J. Mol. Sci.*, 2021, **22**, 1742.
19 M. Wang, E. R. Sampson, H. Jin, J. Li, Q. H. Ke, H.-J. Im and D. Chen, *Arthritis Res. Ther.*, 2013, **15**, R5.
20 X. Wang, P. A. Manner, A. Horner, L. Shum, R. S. Tuan and G. H. Nuckolls, *Osteoarthr. Cartil.*, 2004, **12**, 963–973.
21 G. A. Cabral-Pacheco, I. Garza-Veloz, C. Castruita-De la Rosa, J. M. Ramirez-Acuña, B. A. Perez-Romero, J. F. Guerrero-Rodriguez, N. Martinez-Avila and M. L. Martinez-Fierro, *Int. J. Mol. Sci.*, 2020, **21**, 9739.

22 M.-P. Hellio Le Graverand-Gastineau, *Osteoarthr. Cartil.*, 2009, **17**, 1393–1401.
23 R. Renkiewicz, L. Qiu, C. Lesch, X. Sun, R. Devalaraja, T. Cody, E. Kaldjian, H. Welgus and V. Baragi, *Arthritis rheum.*, 2003, **48**, 1742–1749.
24 A. Gimeno, R. Beltrán-Debón, M. Mulero, G. Pujadas and S. Garcia-Vallvé, *Drug Discovery Today*, 2020, **25**, 38–57.
25 S. K. Baidya, S. Banerjee, N. Adhikari and T. Jha, *J. Med. Chem.*, 2022, **65**, 10709–10754.
26 X.-W. Xie, R.-Z. Wan and Z.-P. Liu, *ChemMedChem*, 2017, **12**, 1157–1168.
27 J. Y. Choi, R. Fuerst, A. M. Knapinska, A. B. Taylor, L. Smith, X. Cao, P. J. Hart, G. B. Fields and W. R. Roush, *J. Med. Chem.*, 2017, **60**, 5816–5825.
28 D. Piecha, J. Weik, H. Kheil, G. Becher, A. Timmermann, A. Jaworski, M. Burger and M. W. Hofmann, *Inflamm. Res.*, 2010, **59**, 379–389.
29 A. M. Bendele, M. Neelagiri, V. Neelagiri and I. Sucholeiki, *Eur. J. Med. Chem.*, 2021, **224**, 113666.
30 V. M. Baragi, G. Becher, A. M. Bendele, R. Biesinger, H. Bluhm, J. Boer, H. Deng, R. Dodd, M. Essers, T. Feuerstein, B. M. Gallagher Jr., C. Gege, M. Hochgürtel, M. Hofmann, A. Jaworski, L. Jin, A. Kiely, B. Korniski, H. Kroth, D. Nix, B. Nolte, D. Piecha, T. S. Powers, F. Richter, M. Schneider, C. Steeneck, I. Sucholeiki, A. Taveras, A. Timmermann, J. Van Veldhuizen, J. Weik, X. Wu and B. Xia, *Arthritis rheum.*, 2009, **60**, 2008–2018.
31 A. R. Johnson, A. G. Pavlovsky, D. F. Ortwine, F. Prior, C.-F. Man, D. A. Bornemeier, C. A. Banotai, W. T. Mueller, P. McConnell, C. Yan, V. Baragi, C. Lesch, W. H. Roark, M. Wilson, K. Datta, R. Guzman, H.-K. Han and R. D. Dyer, *J. Biol. Chem.*, 2007, **282**, 27781–27791.
32 S. J. Taylor, A. Abeywardane, S. Liang, I. Muegge, A. K. Padyana, Z. Xiong, M. Hill-Drzewi, B. Farmer, X. Li, B. Collins, J. X. Li, A. Heim-Riether, J. Proudfoot, Q. Zhang, D. Goldberg, L. Zuvela-Jelaska, H. Zaher, J. Li and N. A. Farrow, *J. Med. Chem.*, 2011, **54**, 8174–8187.
33 P. Song, Z. Cui and L. Hu, *J. Controlled Release*, 2022, **352**, 946–960.
34 M. C. Cristiano, A. Mancuso, E. Giuliano, D. Cosco, D. Paolino and M. Fresta, *J. Funct. Biomater.*, 2021, **12**, 34.
35 C. H. Evans, V. B. Kraus and L. A. Setton, *Nat. Rev. Rheumatol.*, 2014, **10**, 11–22.
36 I. A. Jones, R. Togashi, M. L. Wilson, N. Heckmann and C. T. Vangsness, *Nat. Rev. Rheumatol.*, 2019, **15**, 77–90.
37 S. Perni and P. Prokopovich, *J. Mater. Chem. B*, 2020, **8**, 5096–5108.
38 Y. P. Singh, J. C. Moses, N. Bhardwaj and B. B. Mandal, *J. Mater. Chem. B*, 2018, **6**, 5499–5529.
39 P. Patil, S. Nene, S. Shah, S. B. Singh and S. Srivastava, *Drug Delivery Transl. Res.*, 2023, **13**, 531–546.
40 T. A. Holland and A. G. Mikos, *J. Controlled Release*, 2003, **86**, 1–14.
41 T. Siefen, S. Bjerregaard, C. Borglin and A. Lamprecht, *J. Controlled Release*, 2022, **348**, 745–759.
42 H. Chattopadhyay, B. Auddy, T. Sur, S. Sana and S. Datta, *J. Mater. Chem. B*, 2016, **4**, 4470–4481.
43 M. C. Bruno, M. C. Cristiano, C. Celia, N. d'Avanzo, A. Mancuso, D. Paolino, J. Wolfram and M. Fresta, *ACS Nano*, 2022, **16**, 19665–19690.
44 M. Chen, P. Yu, J. Xing, Y. Wang, K. Ren, G. Zhou, J. Luo, J. Xie and J. Li, *J. Mater. Chem. B*, 2022, **10**, 4479–4490.
45 A. Sulistio, F. Reyes-Ortega, A. M. D'Souza, S. M. Y. Ng, D. Valade, J. F. Quinn, A. C. Donohue, F. Mansfeld, A. Blencowe, G. Qiao, R. Prankerd, S. Quirk, M. R. Whittaker, T. P. Davis and R. J. Tait, *J. Mater. Chem. B*, 2017, **5**, 6221–6226.
46 A. R. Tellegen, I. Rudnik-Jansen, L. Utomo, S. Versteeg, M. Beukers, R. Maarschalkerweerd, D. van Zuilen, N. J. van Klaveren, K. Houben, E. Teske, P. R. van Weeren, N. Karssemakers-Degen, G. Mihov, J. Thies, N. Eijkelkamp, L. B. Creemers, B. P. Meij and M. A. Tryfonidou, *Osteoarthr. Cartil.*, 2023, **31**, 351–362.
47 L. Pang, H. Jin, Z. Lu, F. Xie, H. Shen, X. Li, X. Zhang, X. Jiang, L. Wu, M. Zhang, T. Zhang, Y. Zhai, Y. Zhang, H. Guan, J. Su, M. Li and J. Gao, *Adv. Healthcare Mater.*, 2023, **12**, 2300315.
48 D. Bicho, S. Ajami, C. Liu, R. L. Reis and J. M. Oliveira, *J. Mater. Chem. B*, 2019, **7**, 1027–1044.
49 Z. Wang, R. Li and J. Zhang, *Adv. Compos. Hybrid Mater.*, 2022, **5**, 2921–2935.
50 S. Mura, J. Nicolas and P. Couvreur, *Nat. Mater.*, 2013, **12**, 991–1003.
51 N. Joshi, J. Yan, S. Levy, S. Bhagchandani, K. V. Slaughter, N. E. Sherman, J. Amirault, Y. Wang, L. Riegel, X. He, T. S. Rui, M. Valic, P. K. Vemula, O. R. Miranda, O. Levy, E. M. Gravallese, A. O. Aliprantis, J. Ermann and J. M. Karp, *Nat. Commun.*, 2018, **9**, 1275.
52 L. He, D. Fan, W. Liang, Q. Wang and J. Fang, *ACS Appl. Bio Mater.*, 2020, **3**, 3276–3284.
53 L. Chen, D. Yan, N. Wu, Q. Yao, H. Sun, Y. Pang and Y. Fu, *Bioactive Mater.*, 2021, **6**, 3062–3073.
54 J. Thomas, V. Chopra, A. Sharma, V. Panwar, S. Kaushik, S. Rajput, M. Mittal, R. Guha, N. Chattopadhyay and D. Ghosh, *Int. J. Biol. Macromol.*, 2021, **190**, 474–486.
55 A. Sharma, V. Panwar, J. Thomas, V. Chopra, H. S. Roy and D. Ghosh, *Colloids Surf., B*, 2021, **200**, 111572.
56 A. Sharma, V. Panwar, V. Chopra, J. Thomas, S. Kaushik and D. Ghosh, *ACS Appl. Nano Mater.*, 2019, **2**, 5483–5491.
57 A. Vyawahare, R. Prakash, C. Jori, A. Ali, S. S. Raza and R. Khan, *ACS Nano*, 2022, **16**, 18579–18591.
58 V. Chopra, J. Thomas, A. Sharma, V. Panwar, S. Kaushik, S. Sharma, K. Porwal, C. Kulkarni, S. Rajput, H. Singh, K. Jagavelu, N. Chattopadhyay and D. Ghosh, *ACS Biomater. Sci. Eng.*, 2020, **6**, 6710–6725.
59 Z. Wang, R. Li and J. Zhang, *Adv. Compos. Hybrid Mater.*, 2022, **5**, 2921–2935.
60 J. E. Kim, D. Song, S. H. Kim, Y. Jung and S. J. Kim, *PLoS One*, 2018, **13**, e0194288.
61 P. Kothari, S. Sinha, A. Sardar, A. K. Tripathi, A. Girme, S. Adhikary, R. Singh, R. Maurya, P. R. Mishra, L. Hingorani and R. Trivedi, *Food Funct.*, 2020, **11**, 8273–8285.

62 J. Zhang, B. Fu, X. Chen, D. Chen and H. Yang, *Exp. Ther. Med*, 2020, **19**, 232–240.
63 V. Neugebauer, J. S. Han, H. Adwanikar, Y. Fu and G. Ji, *Mol. Pain*, 2007, **3**, 1744–8069.
64 Y. Luo, J. Li, B. Wang, Q. Zhang, Y. Bian and R. Wang, *J. Bioenerg. Biomembr.*, 2021, **53**, 285–293.
65 S.-J. Kang, J.-W. Kim, K.-Y. Kim, S.-K. Ku and Y.-J. Lee, *J. Orthop. Surg. Res.*, 2014, **9**, 14.
66 I.-J. Chen and C.-S. Wong, *Nutrients*, 2020, **12**, 957.
67 S. Sharma, K. Porwal, C. Kulkarni, S. Pal, P. Sihota, S. Kumar, M. Chandra Tiwari, R. Katekar, A. Kumar, P. Singh, S. Rajput, R. Guha, N. Kumar, J. R. Gayen and N. Chattopadhyay, *Food Funct.*, 2022, **13**, 2184–2199.
68 K. P. H. Pritzker, S. Gay, S. A. Jimenez, K. Ostergaard, J.-P. Pelletier, P. A. Revell, D. Salter and W. B. van den Berg, *Osteoarthr. Cartil.*, 2006, **14**, 13–29.
69 H. Liu, J. Ding, J. Wang, Y. Wang, M. Yang, Y. Zhang, F. Chang and X. Chen, *PLoS One*, 2015, **10**, e0120596.
70 H. S. Roy, N. K. M. S. Rajput, S. Sadhukhan, V. Gowri, A. H. Dar, M. Monga, N. Salaria, R. Guha, N. Chattopadhyay, G. Jayamurugan and D. Ghosh, *Chem. – Eur. J.*, 2023, **29**(53), e202301748.
71 A. Haseeb, D. Chen and T. M. Haqqi, *Rheumatology*, 2013, **52**, 998–1008.
72 R. Largo, M. A. Alvarez-Soria, I. Díez-Ortego, E. Calvo, O. Sánchez-Pernaute, J. Egido and G. Herrero-Beaumont, *Osteoarthr. Cartil.*, 2003, **11**, 290–298.
73 H. Yi, W. Zhang, Z.-M. Cui, S.-Y. Cui, J.-B. Fan, X.-H. Zhu and W. Liu, *J. Orthop. Surg. Res.*, 2020, **15**, 1–9.
74 L. Zhang, S. Ma, H. Su and J. Cheng, *Mol. Ther. Methods Clin. Dev.*, 2018, **9**, 153–159.
75 D. Bizzoca, L. Moretti, A. Gnoni, F. L. Moretti, S. Scacco, G. Banfi, A. Piazzolla, G. Solarino and B. Moretti, *J. Funct. Morphol. Kinesiol.*, 2022, **7**, 97.
76 M. Thing, N. Mertz, L. Ågårdh, S. W. Larsen, J. Østergaard and C. Larsen, *J. Drug Delivery Sci. Technol.*, 2019, **49**, 169–176.
77 A. Ahmad, M. Irshad, W. Ahmad, A. Khan and R. Ahmad, *J. Med. Biochem.*, 2011, **30**, 15–24.
78 Y. Yoshihara, H. Nakamura, K. Obata, H. Yamada, T. Hayakawa, K. Fujikawa and Y. Okada, *Ann. Rheum. Dis.*, 2000, **59**, 455–461.
79 X. Xin, Q. Tan, F. Li, Z. Chen, K. Zhang, F. Li, B. Yang, Z. Xing, F. Zhou, Y. Tian, Y. Lv and T. Zhu, *Front. Surg.*, 2021, **8**, DOI: **10.3389/fsurg.2021.750047**.
80 M. L. Ferrándiz, M. C. Terencio, R. Ruhí, J. Vergés, E. Montell, A. Torrent and M. J. Alcaraz, *Exp. Gerontol.*, 2014, **55**, 44–48.
81 A. Gigout, D. Harazin, L. M. Topping, D. Merciris, S. Lindemann, C. Brenneis and A. Nissim, *Arthritis Res. Ther.*, 2021, **23**, 113.
82 L. Ma, J. Wu and Q. H. Jin, *Mol. Med. Rep.*, 2017, **16**, 8799–8807.
83 J. Pan, X. Zhou, W. Li, J. E. Novotny, S. B. Doty and L. Wang, *J. Orthop. Res.*, 2009, **27**, 1347–1352.
84 N. Aizah, P. P. Chong and T. Kamarul, *Cartilage*, 2021, **13**, 1322S–1333S.
85 M. Pickarski, T. Hayami, Y. Zhuo and L. T. Duong, *BMC Musculoskeletal Disord.*, 2011, **12**, 197.
86 K. Arakawa, K. Takahata, S. Enomoto, Y. Oka, K. Ozone, S. Nakagaki, K. Murata, N. Kanemura and T. Kokubun, *Osteoarthr. Cartil.*, 2022, **30**, 451–460.
87 S. R. Goldring, *Med. Clin. North Am.*, 2009, **93**, 25–35.
88 T. Neogi, M. Nevitt, J. Niu, L. Sharma, F. Roemer, A. Guermazi, C. E. Lewis, J. Torner, K. Javaid and D. Felson, *Ann. Rheum. Dis.*, 2010, **69**, 841–844.
89 R. Molthen, J. Jameson, C. Albert, P. Smith and G. Harris, *Transitional Care in Osteogenesis Imperfecta: Advances in Biology, Technology and Clinical Practice*, 1st edn, 2015, ch. 12, pp. 195–216.
90 K. Nganvongpanit, B. Boonsri, T. Sripratak and P. Markmee, *J. Vet. Sci.*, 2013, **14**, 215.
91 Z. Zhang, L. Li, W. Yang, Y. Cao, Y. Shi, X. Li and Q. Zhang, *Osteoarthr. Cartil.*, 2017, **25**, 309–320.

